

Total Cross Sections for Neutron Scattering

C.R. Chinn^{(a),(b)}, Ch. Elster^(c), R.M. Thaler^{(a),(d)}, and
S.P. Weppner^(c).

^(a) *Department of Physics and Astronomy, Vanderbilt University, Nashville, TN 37235*

^(b) *Center for Computationally Intensive Physics, Oak Ridge National Laboratory,
Oak Ridge, TN 37831*

^(c) *Institute of Nuclear and Particle Physics, and Department of Physics,
Ohio University, Athens, OH 45701*

^(d) *Physics Department, Case Western Reserve University, Cleveland, OH 44106.*

(Received February 9, 2008)

PACS: 25.40.Cm

ABSTRACT

Measurements of neutron total cross-sections are both extensive and extremely accurate. Although they place a strong constraint on theoretically constructed models, there are relatively few comparisons of predictions with experiment. The total cross-sections for neutron scattering from ^{16}O and ^{40}Ca are calculated as a function of energy from 50 – 700 MeV laboratory energy with a microscopic first order optical potential derived within the framework of the Watson expansion. Although these results are already in qualitative agreement with the data, the inclusion of medium corrections to the propagator is essential to correctly predict the energy dependence given by the experiment. In the region between 100 and 200 MeV, where off-shell $t\rho$ calculations for both ^{16}O and ^{40}Ca overpredict the experiment, the modification due to the nuclear medium reduces the calculated values. Above 300 MeV these corrections are very small and depending on the employed nuclear mean field tend to compensate for the underprediction of the off-shell $t\rho$ results.

Accurate measurements of total cross-sections for the scattering of neutrons from a variety of nuclei provide stringent constraints on theoretical models. In this sense one would like to incorporate a realistic physical description of the nucleon-nucleon [NN] interaction, which quantitatively reproduces the NN observables, including the total neutron cross-section, into a theoretical model of neutron-nucleus scattering. Such a description would ideally result from multiple scattering theory and the use the NN interaction together with nuclear wave functions as input to obtain nucleon-nucleus observables. In a recent publication [1] we presented a microscopic treatment of the modification of the NN propagator due to the nuclear medium, formulated to be consistent with the first order spectator expansion [2,3]. Calculations of proton and neutron elastic scattering from ^{40}Ca in the first order spectator expansion were presented, in which the effect of the nuclear medium was taken into account. These results were very encouraging. In particular, the neutron total cross-section for scattering from ^{40}Ca was shown as a function of energy. It was gratifying to observe [1] that the effect of the nuclear medium, although not large, lowered (relative to those for which a free NN t-matrix was employed) the calculated values in the energy regime between 100 and 300 MeV and brought the theoretical predictions into closer agreement with the measured values. Furthermore, above ~ 400 MeV, where the ‘free’ predictions fell below the experimental data, the medium correction raised the predicted values, so that in this region a better description of the experiment was also achieved. The comparisons shown in Ref. [1] were limited to the scattering of neutrons from ^{40}Ca , and it was felt that it would be reassuring to extend the calculation to other targets. At present the calculations are limited to spin-saturated even-even targets and so only the scattering from ^{16}O and ^{40}Ca are investigated here.

In this work the full Bonn potential [4] is used to calculate the $H(n, p)$ total cross-sections for projectile energies less than 350 MeV. This interaction includes the effects of relativistic kinematics, retarded meson propagators as given by time-ordered perturbation theory, and crossed and iterative meson exchanges with NN , $N\Delta$ and $\Delta\Delta$ intermediate states. For energies greater than 350 MeV a less sophisticated high energy extension of the

Bonn potential [5] is used, which incorporates the effects of pion production via $N\Delta$ and $\Delta\Delta$ iterative diagrams.

The calculations for nuclei other than ^1H are performed in the parameter-free manner as outlined in Ref. [1], where the only inputs are the free NN interaction, target nuclear densities and the static mean field potential used to model the medium effects. The free NN t-matrix is taken from the same Bonn potential that is used to calculate the $\text{H}(n, p)$ result. The nuclear mean field potentials are taken from a Hartree-Fock-Bogolyubov (HFB) microscopic nuclear structure calculation, which utilizes the density-dependent finite-ranged *Gogny D1S* effective NN interaction [6,7]. A second choice involves a nonrelativistic reduction of the mean field potentials resulting from a Dirac-Hartree (DH) calculation based upon the σ - ω model [8]. The neutron-nucleus calculations are performed in an ‘off-shell $t\rho$ ’ framework using the optimum factorized form as described in Ref. [9], where the fully off-shell effective NN t-matrix is used, but with diagonal nuclear densities.

For a comparison with two-nucleon scattering, in Fig. 1 the total cross-section for neutron-proton (np) scattering is shown. The solid line represents the experimental data [10], while the diamonds represent the predictions from the full Bonn interaction [4]. It should be noted that, although these data were not included in the fitting procedure for the Bonn potential, excellent agreement is obtained. Included in Fig. 1 are the predictions for the neutron-neutron (nn) total cross-section, which are obtained by considering only the $T=1$ partial waves. No data are given for this case, since none exist. However, the excellent agreement with the (n, p) experimental data suggests that the (n, n) predictions are likewise reliable.

In Fig. 2 the total neutron cross-section data for scattering from ^{16}O and ^{40}Ca are presented as a function of the neutron laboratory energy. Note that for ^{16}O in the upper panel of Fig. 2 the corrections due to the nuclear medium are small, but tend in the correct direction. At lower energies (100 – 200 MeV), these medium effects reduce the calculated cross-section in comparison to the free result and bring the predictions into rather good agreement with the measured values. At higher energies the effect of the coupling of the

struck nucleon to the rest of the nucleus tends to increase the total cross-section value slightly to again yield a result which is closer to the data. The analogous result for ^{40}Ca is shown in the lower panel of Fig. 2, and as described for ^{16}O , the contributions due the propagator modification by the nuclear medium tend to improve the description of the experimental observable.

If one were to assume that there were no shadowing effect then one would expect the total neutron cross-sections to scale with the number of nucleons, A . In this case the isospin averaged $\langle\sigma_T\rangle$ of the (n, p) and (n, n) cross-sections shown in Fig. 1 multiplied by $A = 16$ and by $A = 40$ are indicated by asterisks in the upper and lower panels of Fig. 2, respectively. These points would represent the energy dependent total cross-sections in the absence of shadowing and thus correspond to an upper limit on the possible values of the total cross-sections. However, the measured values for ^{16}O and ^{40}Ca are indeed of the order of 25%–30% smaller than this limiting value, and one should expect any microscopic treatment to be closer than this limit. The horizontal arrows indicate the geometric black disk cross-section $2\pi R^2$ (with $R = \frac{5}{3}\langle r_{rms}\rangle$). For energies for which the total cross-section exceeds this geometric limit, one should be very skeptical of the first-order multiple scattering theory. For ^{16}O this energy is roughly 50 MeV and for ^{40}Ca it is about 70 MeV.

Although the ^{16}O and ^{40}Ca results do not scale as $A \times \langle\sigma_T\rangle$, they may scale for some effective number of nucleons, A_{eff} . In this sense one can partially account for shadowing. In Fig. 3 the average neutron-nucleon total cross-section, $\langle\sigma_T\rangle$ is plotted along with the the ^{16}O and ^{40}Ca results divided by A_{eff} . In this case $A_{eff} \approx 12$ and $A_{eff} \approx 26$ for ^{16}O and ^{40}Ca , respectively. The ^{16}O and ^{40}Ca experimental measurements scale remarkably well for energies greater than about 80 MeV. For the high energies where scaling is occurring it seems clear one is basically observing effects due to the NN interaction. Contributions beyond the first order multiple scattering theory are not so important in this regime. It is also true that this may be an indication that the total cross-section data is less revealing than angular measurements. For smaller energies the break down of scaling illustrates how higher order corrections to the first order theory are required.

In Fig. 4 the total elastic cross-sections σ_{el} and the total reaction cross-sections σ_R for ^{16}O are displayed separately. Since the reaction cross-section is considerably larger than the elastic cross-section for laboratory kinetic energies greater than 100 MeV, it follows that the corrections to the total cross-section due to the nuclear medium are largely given by contributions to the reaction cross-sections. The same conclusion can be made about the ^{40}Ca elastic and reaction cross-sections. Qualitatively the observed effect of the medium may be interpreted as follows. Since the interactions between the struck nucleon and the ‘residual (A-1) nucleus’ is attractive, the medium correction in a sense tends to reduce the knock-out probability for outer nucleons, thus reducing the reaction cross-section. This is particularly the case for energies lower than 200 MeV, where the scattering process is expected to be surface dominated. At higher energies, the projectile neutron penetrates more deeply into the nucleus, so that this effect becomes less important.

To demonstrate that contributions due to the nuclear medium can be significant in neutron elastic scattering, the neutron differential cross-section, the analyzing power and the spin rotation parameter for scattering from ^{16}O at 100 and 500 MeV are shown in Figs. 5 and 6. At higher energies the corrections do not begin to manifest themselves until the scattering angles become so large that higher order processes need to be taken into account. At the lower energy there is certainly a significant difference in the spin observables even at small angles.

In conclusion the precision neutron total cross-section measurements provide another striking confirmation that the first order theory of the optical potential can accurately describe data in the appropriate regime of applicability. These successes encourage us to proceed in this direction and in the future to include higher order contributions in the multiple scattering spectator expansion.

ACKNOWLEDGMENTS

The authors would like to thank R.W. Finlay and J. Rapaport for many discussions concerning this work. The computational support of the the Ohio Supercomputer Center under Grants No. PHS206 and PDS150 is gratefully acknowledged. This work was performed in part under the auspices of the U. S. Department of Energy under contracts No. DE-FG02-93ER40756 with Ohio University, DE-AC05-84OR21400 with Martin Marietta Energy Systems, Inc., and DE-FG05-87ER40376 with Vanderbilt University. This research has also been supported in part by the U.S. Department of Energy, Office of Scientific Computing under the High Performance Computing and Communications Program (HPCC) as a Grand Challenge titled the Quantum Structure of Matter.

REFERENCES

- [1] C.R. Chinn, Ch. Elster, and R.M. Thaler, Phys. Rev. **C48** 2956 (1993).
- [2] A. Picklesimer and R. M. Thaler, Phys. Rev. **C 23**, 42 (1981).
- [3] E. R. Siciliano and R. M. Thaler, Phys. Rev. **C 16**, 1322 (1977).
- [4] R. Machleidt, K. Holinde, and Ch. Elster, Phys. Rep. **149**, (1987).
- [5] Ch. Elster and P.C. Tandy, Phys. Rev. **C40** (1989), 881; Ch. Elster, Ph.D. thesis, University of Bonn, 1986.
- [6] See for example J.F. Berger, M. Girod, and D. Gogny, Nucl. Phys. **A502**, 85c (1989); J.P. Delaroche, M. Girod, J. Libert and I. Deloncle, Phys. Lett. **B232**, 145 (1989).
- [7] J.F. Berger, M. Girod, and D. Gogny, Comput. Phys. Commun. **63**, 365 (1991).
- [8] Horowitz and B. Serot, Nucl. Phys **A368**, 503 (1981).
- [9] A. Picklesimer, P.C. Tandy, R.M. Thaler and D.H. Wolfe, Phys. Rev. **C30**, 2225 (1984).
- [10] P.W. Lisowski et *al.*, Phys. Rev. Lett. **49**, 255 (1982).
- [11] R. W. Finlay, W. P. Abfalterer, G. Fink, E. Montei, T Adami, P. W. Lisowski, G. L. Morgan and R. C. Haight, Phys. Rev. **C 47**, 237 (1993).
- [12] R.W. Finlay, G. Fink, W. Abfalterer, P. Lisowski, G.L. Morgan, and R.C. Haight, in *Proceedings of the Internat. Conference on Nuclear Data for Science and Technology*, edited by S.M. Qaim (Springer-Verlag, Berlin, 1992), p. 702.

FIGURES

FIG. 1. The total cross-section σ_{tot} for the scattering of neutrons from protons $H(n, p)$ is shown. The solid curve corresponds to the experimental data [10]. No error bars are shown, since the total systematic uncertainty is smaller than 1% and the errors fall within the thickness of the plotted line. The diamonds represent the theoretical predictions from the full Bonn potential, the triangles give the results for the (n, n) case.

FIG. 2. The total neutron-nucleus total cross-sections for scattering from ^{16}O and ^{40}Ca are shown as a function of the incident neutron kinetic energy in the upper and lower panels, respectively. The data are taken from Ref. [11,12]. The circles correspond to the free result, while the squares and triangles include the medium contributions using the DH and HFB mean field potentials, respectively. The calculations below 350 MeV are based on the full Bonn NN t-matrix [4], those above 350 MeV use the high energy extension of the Bonn potential [5] as input. The asterisks represent $A \times \langle \sigma_t \rangle$, where $\langle \sigma_t \rangle$ is the isospin averaged neutron-nucleon total cross-section and A is the atomic number, and the horizontal arrows give the geometric black disk cross section as described in the text.

FIG. 3. The isospin averaged neutron-nucleon total cross-section calculated from the average of the (n, p) and (n, n) results and shown as open circles is compared to the ^{16}O and ^{40}Ca neutron total cross-section measurements divided by A_{eff} . The solid line represents the ^{16}O data divided by $A_{eff} = 12$ and the dashed line the ^{40}Ca data divided by $A_{eff} = 26$.

FIG. 4. The elastic and reaction cross-sections are shown for ^{16}O in the upper and lower panels, respectively. The circles represent the free result, while the squares and triangles include the medium contributions using the DH and HFB mean field potentials, respectively.

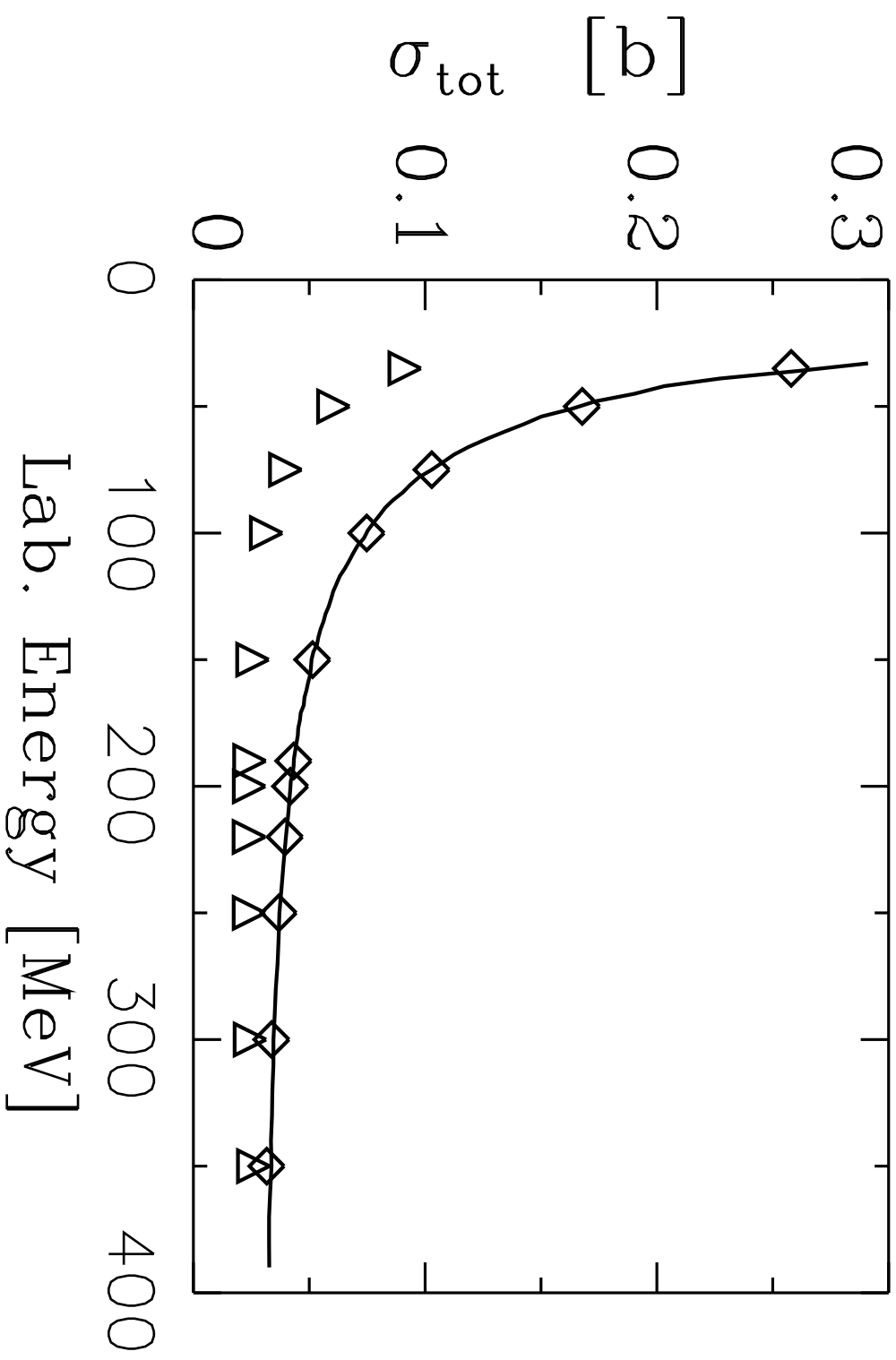
FIG. 5. The angular distribution of the differential cross-section ($\frac{d\sigma}{d\Omega}$), analyzing power (A_y) and spin rotation function (Q) for elastic neutron scattering from ^{16}O at 100 MeV laboratory energy. The calculations are performed with a first-order optical potential obtained from the full Bonn interaction [4] in the optimum factorized form. The solid curve represents the free impulse approximation with using the free NN t-matrix. The medium contributions are included in the dashed curves, where the DH mean potential is used for the dashed-dotted curve and the HFB mean field potential for the dashed curve.

FIG. 6. Same as Fig. 5, except the projectile kinetic energy is 500 MeV.

This figure "fig1-1.png" is available in "png" format from:

<http://arXiv.org/ps/nucl-th/9410030v1>

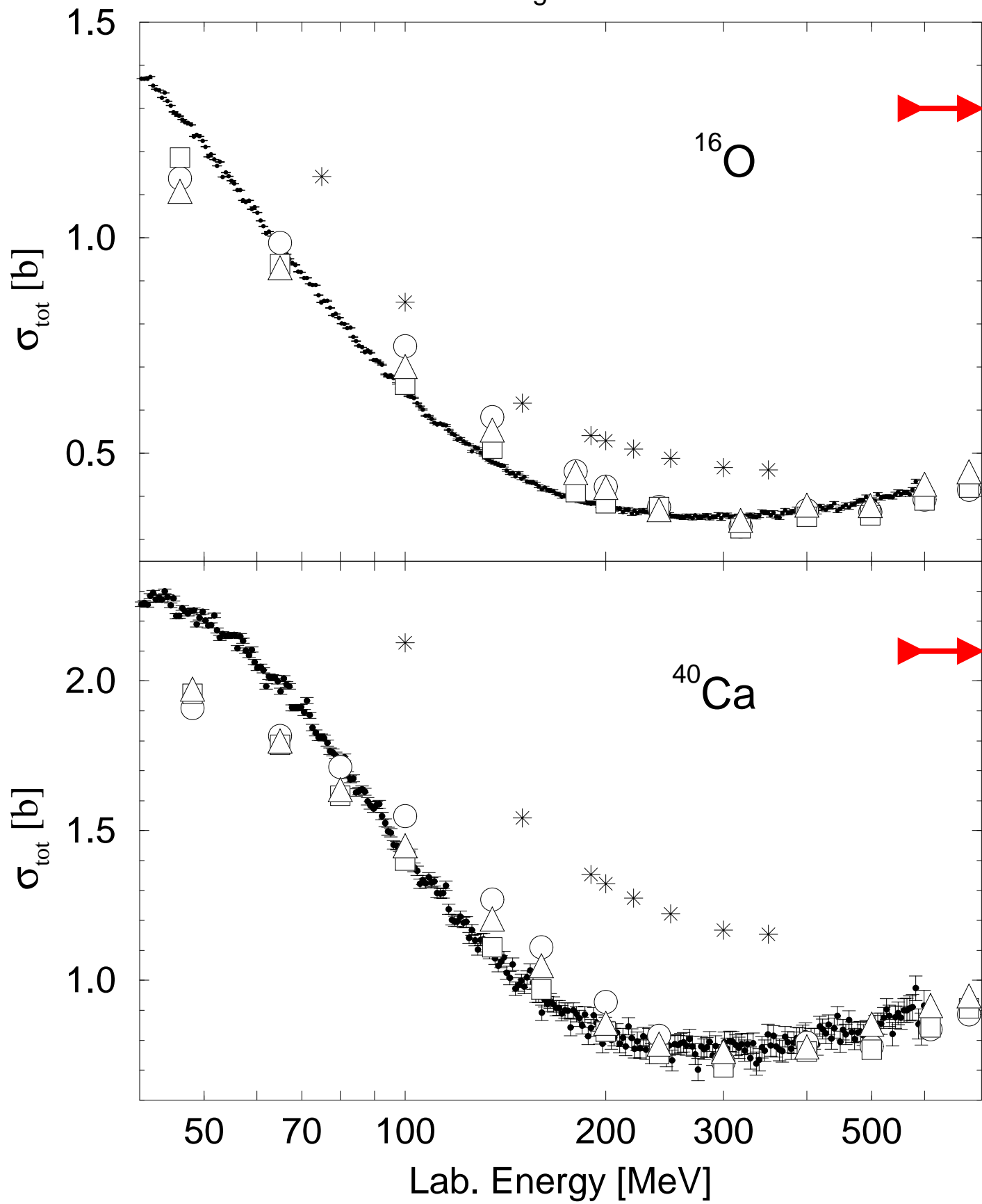
Fig. 1



This figure "fig1-2.png" is available in "png" format from:

<http://arXiv.org/ps/nucl-th/9410030v1>

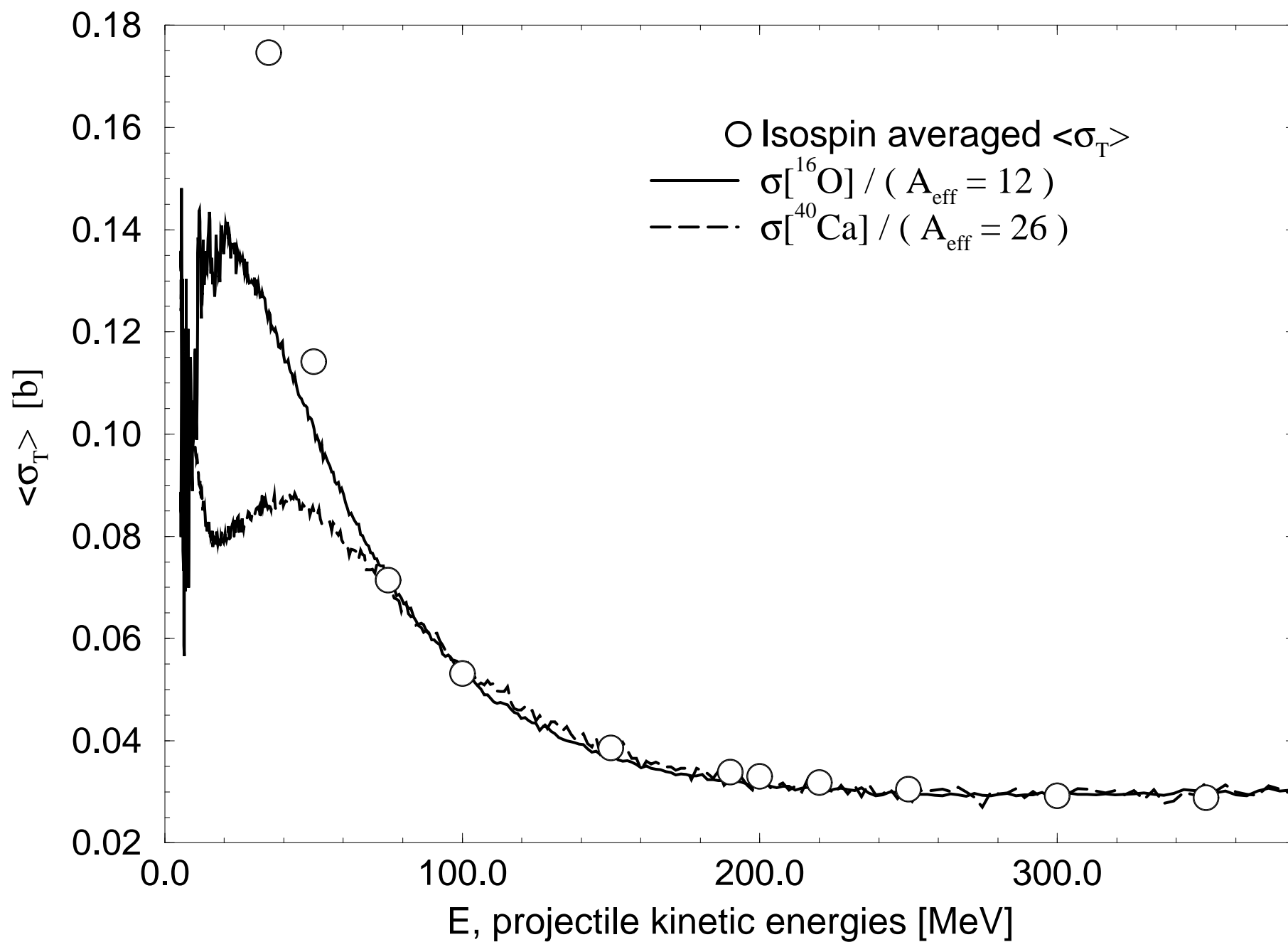
Figure 2



This figure "fig1-3.png" is available in "png" format from:

<http://arXiv.org/ps/nucl-th/9410030v1>

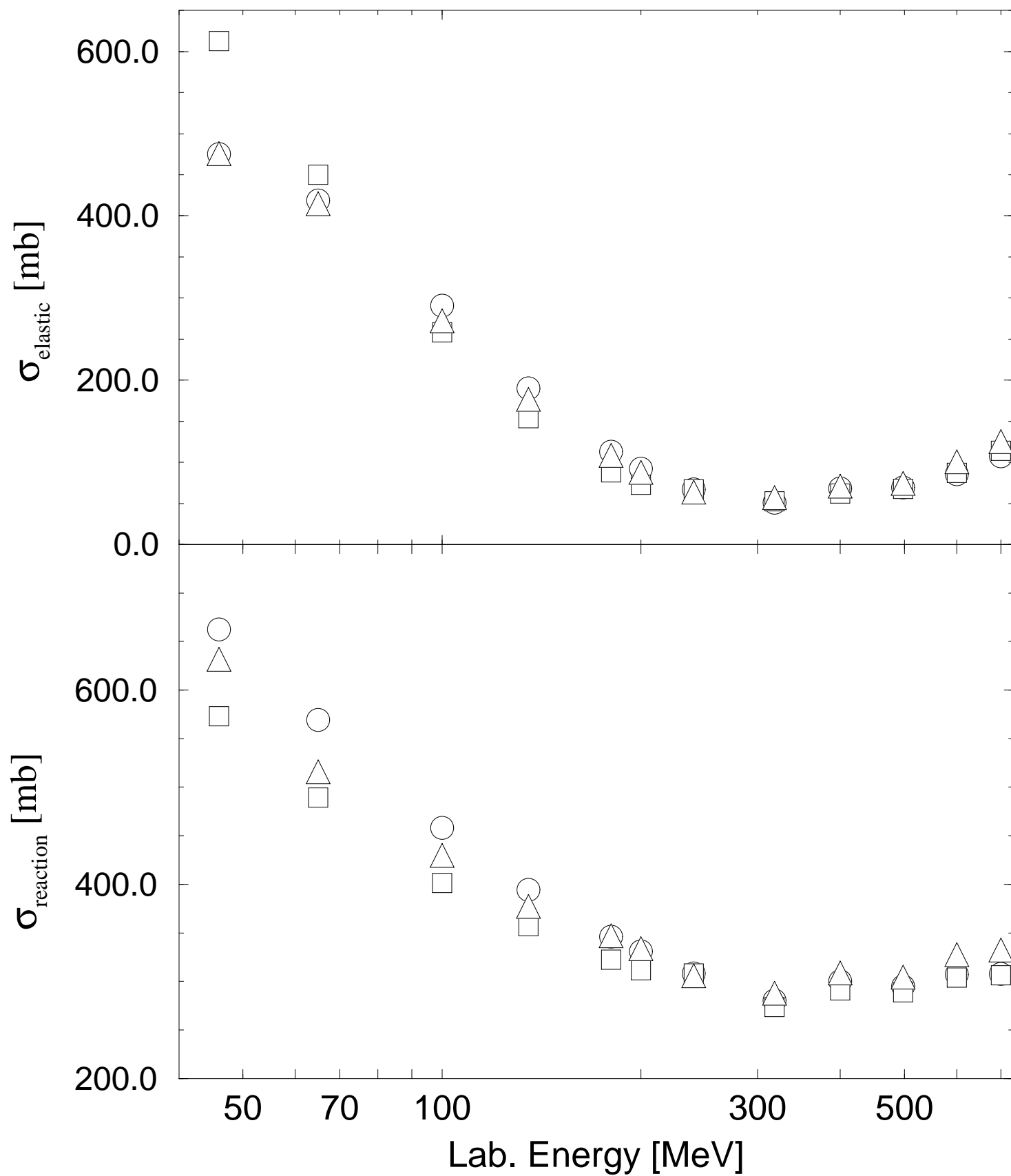
Figure 3



This figure "fig1-4.png" is available in "png" format from:

<http://arXiv.org/ps/nucl-th/9410030v1>

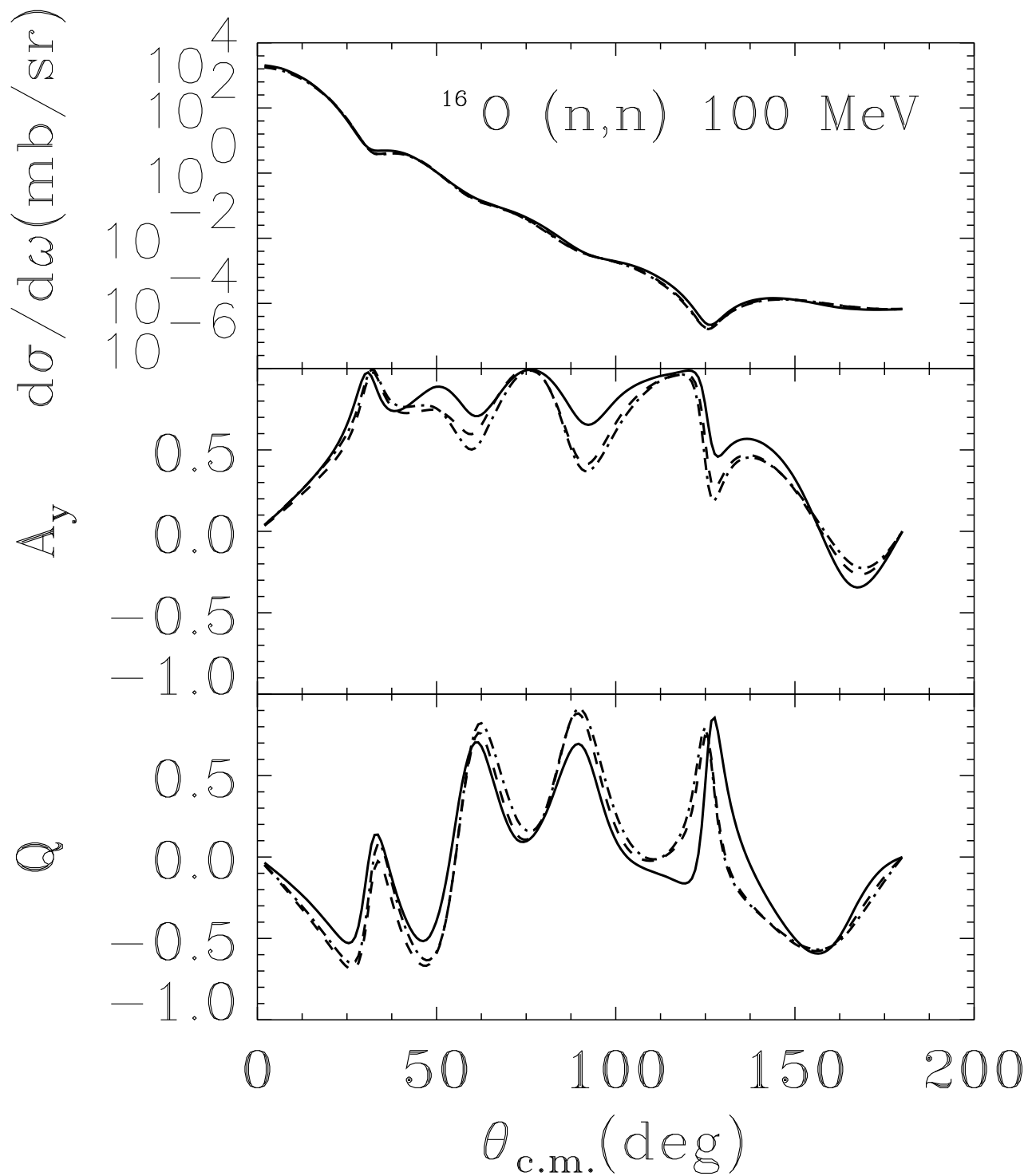
Figure 4



This figure "fig1-5.png" is available in "png" format from:

<http://arXiv.org/ps/nucl-th/9410030v1>

Fig. 5



This figure "fig1-6.png" is available in "png" format from:

<http://arXiv.org/ps/nucl-th/9410030v1>

Fig. 6

